LAWRENCE
LIVERMORE
NATIONAL
LABORATORY

LLNL-TR-432011

Coolant Compatibility Studies for Fusion and Fusion-Fission Hybrid Reactor Concepts: Corrosion of Oxide Dispersion Strengthened Iron-Chromium Steels and Tantalum in High Temperature Molten Fluoride Salts

J. Farmer, B. El-dasher, J. Ferreira, M. Caro, A. Kimura

May 14, 2010

Disclaimer

This work performed under the auspices of the U.S. Department of Energy by Lawrence Livermore National Laboratory under Contract DE-AC52-07NA27344.

Coolant Compatibility Studies for Fusion and Fusion-Fission Hybrid Reactor Concepts: Corrosion of Oxide Dispersion Strengthened Iron-Chromium Steels and Tantalum in High Temperature Molten Fluoride Salts

Joseph Farmer[1], Bassem El-dasher[1], James Ferreira[1], Magdalena Serrano de Caro[1] and Akihiko Kimura[2]

[1]Lawrence Livermore National Laboratory, Livemore, California 94550, USA
[2] Institute of Advanced Energy,Kyoto University, Gokasho, Uji, Kyoto 611-0011, Japan

ABSTRACT

Alloys such as 12YWT & 14YWT have exceptional high-temperature strength at temperatures greater than 550°C. This class of materials has also demonstrated relatively little radiation induced swelling at damage levels of at least 75 dpa in sodium-cooled fast reactors. However, corrosion of oxide dispersion strengthened (ODS) steels in high temperature molten fluoride salts may limit the life of advanced reactor systems, including some fusion and fusion-fission hybrid systems that are now under consideration.

This paper reports corrosion studies of ODS steel in molten fluoride salts at temperatures ranging from 600 to 900°C. Electrochemical impedance spectroscopy (EIS) was used to measure the temperature dependence of charge transfer kinetics *in situ*, while an environmental electron microscope (ESEM) equipped with energy dispersive spectroscopy (EDS) was used for post-exposure examination of test samples. ODS steel experienced corrosion in the molten fluoride salts at 550 to 900°C, even in carefully controlled glove-box environments with very low levels of oxygen and moisture. The observed rate of attack was found to accelerate dramatically at temperatures above 800°C. Tantalum and tantalum-based alloys such as Ta-1W and Ta-10W have exceptional high temperature strength, far better than ODS steels. Unlike ODS steels, tantalum has been found to exhibit some immunity to corrosive attack by molten fluoride salts at temperatures as high as 900°C, though there is some indication that grain boundary attack may have occurred. Unfortunately, tantalum alloys are known to become brittle during irradiation and exposure to hydrogen, both of which are important in fusion applications.

INTRODUCTION

Fusion and fusion-fission hybrid reactors have now been designed to produce nuclear power from natural or depleted uranium without isotopic enrichment, and from spent nuclear fuel from light water reactors without chemical separation into weapons-attractive actinide streams. A point-source of high-energy neutrons produced by laser-generated, thermonuclear fusion within a target is used to achieve ultra-deep burn-up of the fertile or fissile fuel in a sub-critical fission blanket. Fertile fuels including depleted uranium (DU), natural uranium (NatU), spent nuclear fuel (SNF), and thorium (Th) can be used. Fissile fuels such as low-enrichment uranium (LEU), excess weapons plutonium (WG-Pu), and excess highly-enriched uranium (HEU) may be used as well. Based upon preliminary analyses, it is believed that LIFE could help meet worldwide electricity needs in a safe and sustainable manner, while drastically shrinking the nation's and world's stockpile of spent nuclear fuel and excess weapons materials. LIFE takes advantage of the significant advances in laser-based inertial confinement fusion that are taking place at the NIF at LLNL where it is expected that thermonuclear ignition will be achieved in the 2010-2011 timeframe.

Materials for fusion-fission hybrid reactors fall into several broad categories, including: (1) lasers and optics, (2) fusion targets, (3) tungsten first wall, (4) neutron multiplication blanket, (5) sub-critical fission blanket, (6) structural and cladding materials, (7) coolants and/or liquid fuels, (8) reflector, and (9) balance of plant. Issues related to lasers and optics, as well as fusion targets are discussed elsewhere. The LIFE engine's structural challenges include: need for high-temperature strength; resistance to high-temperature creep; immunity to radiation damage, including swelling and helium embrittlement; resistance to corrosion and environmental cracking in high-temperature molten fluoride salts; and the ability to be fabricated into necessary shapes and configurations with practical welding processes. It is hoped that the structural challenges can be met with oxide dispersion strengthened (ODS) ferritic steels [1-5]. This article focuses on the interaction of structural materials with coolants and/or liquid fuels.

Figure 1 – ODS steel samples used in the corrosion study discussed in in this paper were fabricated from the extruded bars shown at the top of this photograph. Rolled sheets have also been made to facilitate joining studies.

Preferred coolants are FLiBe (Li_2BeF_4) in the primary coolant loop and FLiNaBe ($LiNaBeF_4$) in the secondary coolant loop [6-8]. Note that FLiBe is a binary mixture of lithium and beryllium fluorides ($2LiF + BeF_2 = Li_2BeF_4$). The FLiBe input temperature is 620°C and the exit temperature for this design is 680°C. The transmutation of lithium in these coolants produces tritium for the steady stream of fusion targets that must be fed to the LIFE engine, thereby making the system self sufficient in tritium. Unfortunately, this reaction also produces very corrosive hydrofluoric acid species (HF and TF), which can rapidly degrade structural and cladding materials. In the case of homogenous liquid fuels, UF_4 and ThF_4 can be dissolved in these molten salt mixtures.

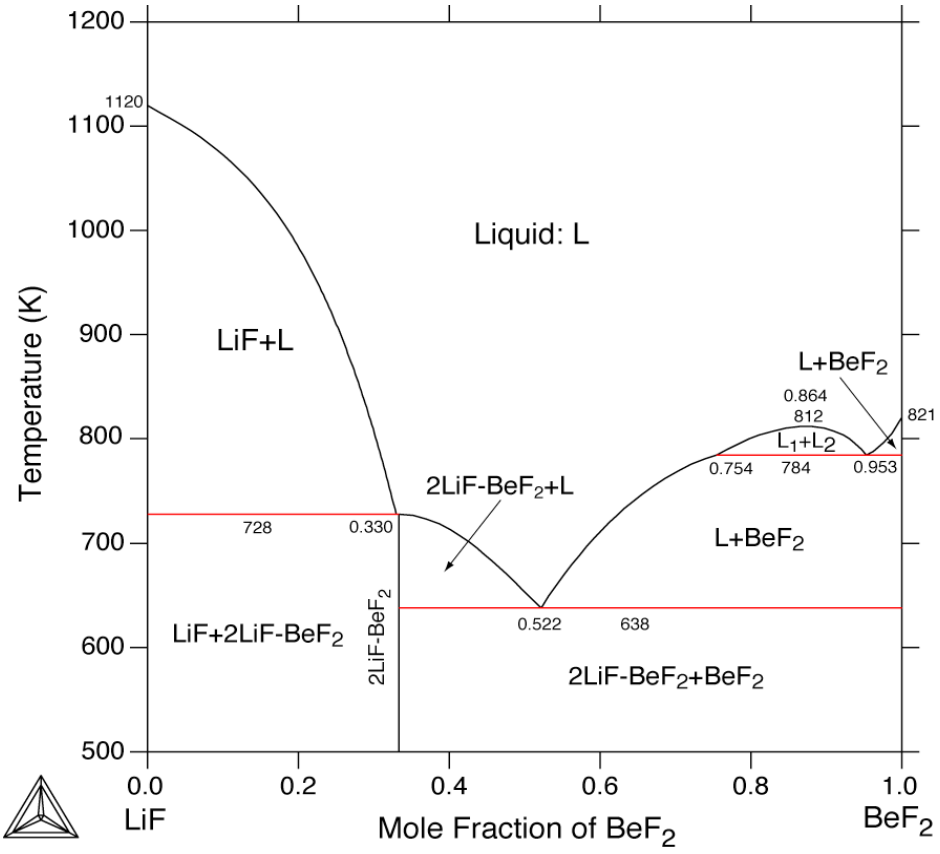

Figure 2 – Molten salt coolants are a mixture of fluoride salts that form low-melting point eutectics (e.g. FLiBe and other compositions).

The relative corrosion susceptibility of refractory metals and Fe-Cr steels can be understood by ranking the free energies of formation for their respective fluoride salts [11]. The transmutation of lithium in the Li_2BeF_4 forms corrosive tritium fluoride, which behaves chemically like hydrogen fluoride, or hydrofluoric acid. Published data indicate that the Cr_2O_3 film provides only limited corrosion protection. The preferential dissolution of chromium into the Li_2Be_4 salt results in the formation of a chromium depletion layer, which lies below a mixed oxide film of $Fe(Fe,Cr)_2O_4$ and disperse deposit of Fe_2O_3 particles [10]. While the presence of metallic beryllium has a positive effect on the formation of corrosive HF (TF), it promotes formation of problematic gaseous BeH_2.

Table 1 – Preferential dissolution of chromium from ODS during molten salt corrosion is not surprising. Mo, W, Ni and V should be stable coatings in molten fluoride salts, while Fe-Cr alloys such as ODS ferritic steel have shown the expected marginal stability.

Fluoride Salts: Possible Corrosion Products	Free Energy of Formation (kcal/g-mol F) at 1000K
MoF_6	-50.2
WF_6	-56.8
NiF_2	-55.3
VF_5	-58
VF_4	-66
HF	-66.2
FeF_2	-66.5
CrF_2	-75.2
BeF_2	-106.9
LiF	-125.2

EXPERIMENTAL

An electrochemical cell developed by LLNL for corrosion testing of structural and cladding materials in high-temperature molten fluoride salts is shown in Figure 3 [12]. The working electrode (larger disk of ODS steel), reference electrode (smaller disk of ODS steel), and counter electrode (platinum bar suspended above the two ODS steel disks). The material being tested is held in the electrochemical by a machined ceramic plug. This figure also shows the cell being operated at 800°C and glowing red-hot. Continued development led to a new electrochemical cell, shown in Figure 4, which was designed to use with crucible furnace in glove box with carefully controlled glove box environment, limiting oxygen and moisture to less that 1 part per million.

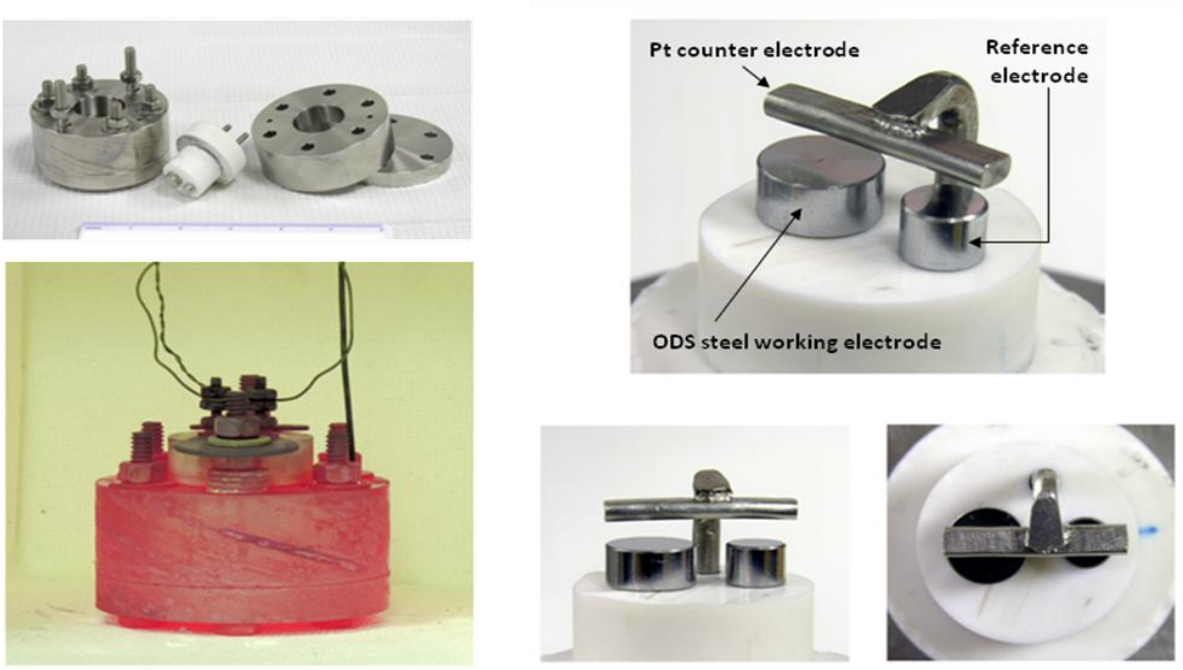

Figure 3 – First high-temperature electrochemical cell designed to enable work with high-temperature molten fluoride salts. This cell enabled several *in situ* measurements: linear polarization; zero resistance ammeter; & electrochemical impedance spectroscopy.

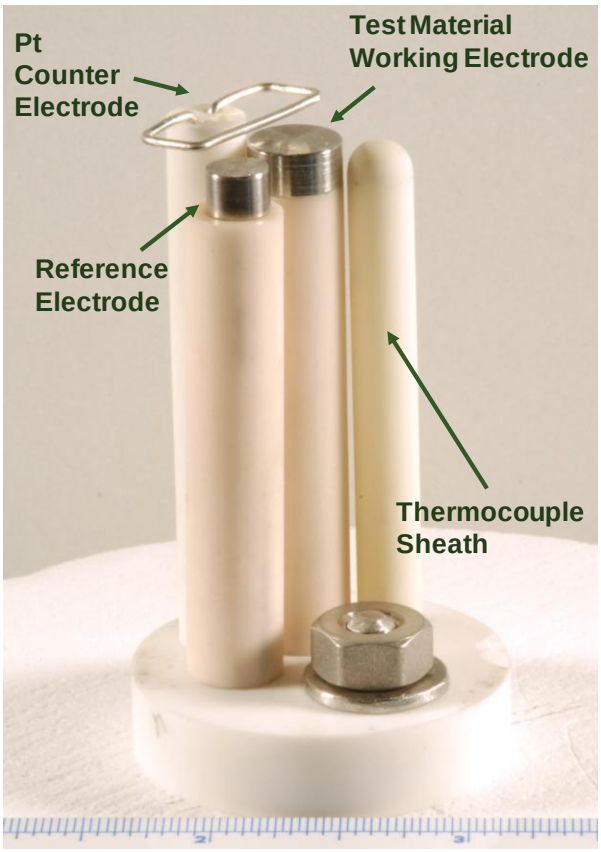

(a)

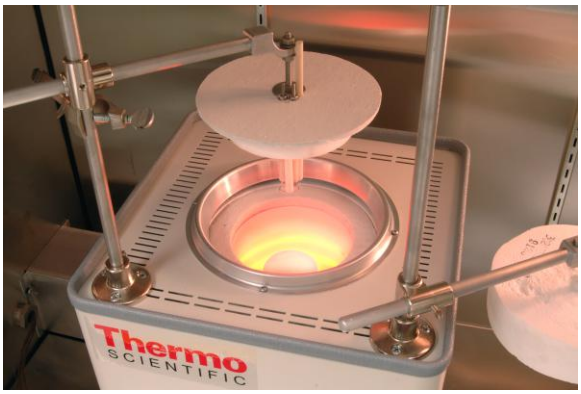

(b)

(c)

Figure 4 – New electrochemical cell designed to use with crucible furnace in glove box with carefully controlled glove box environment, limiting oxygen and moisture to less that 1 part per million.

RESULTS

The corrosive attack of an early ODS steel sample, which is a powder metallurgy product, is shown in Figure 5. The molten salt infiltrated the re-crystallized and damaged surface layer, which had a thickness of approximately 200 microns, and dissolved chromium oxide inclusions within the layer. Improved ODS steels are being developed to eliminate this problem.

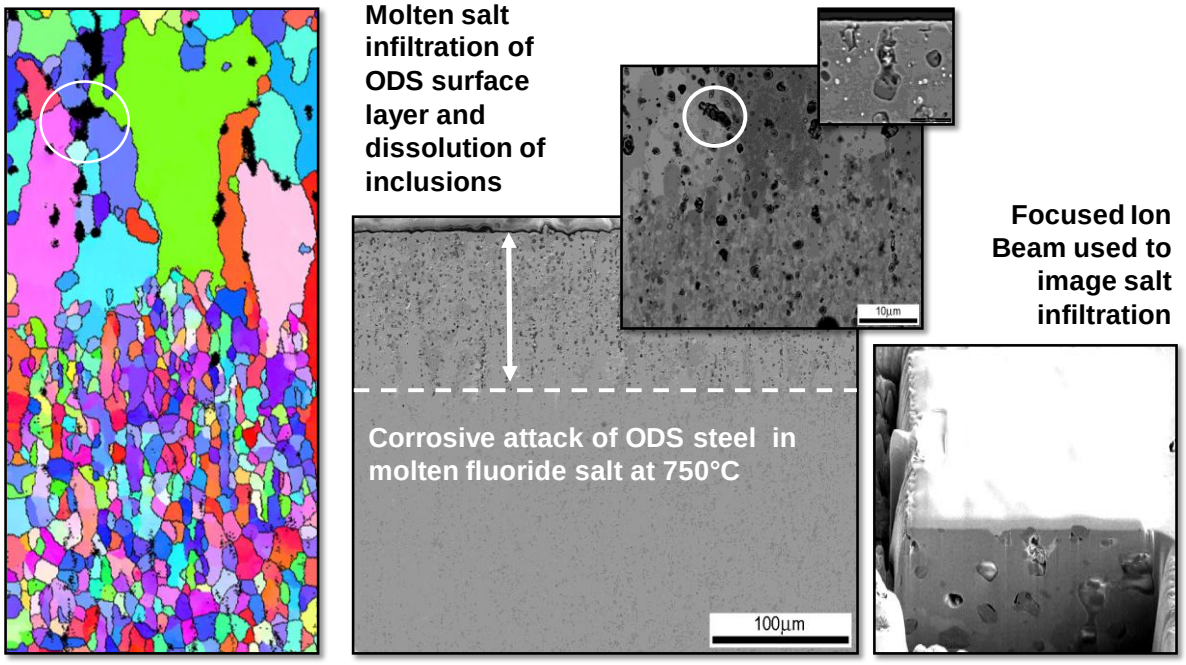

Figure 5 – Realistic corrosion tests of candidate structural materials are already being conducted. Such tests revealed anticipated vulnerabilities quickly. Better performance over years of operation would be surprising.

Electron microscopy of of the ODS-FLiNaK interface has yielded valuable insight into corrosion mechanisms, and temperature-dependent changes in those mechanisms (Figure 6). Dramatic increases in corrosion occur above 800°C. The corrosion of Kyoto University alloys K3, K5 & K6 in molten fluoride salt (FLiNaK) were also studied (Figure 7). These images were obtained after EIS at 600°C, and show mild corrosion at this temperature, with polishing marks still evident. The corrosion of Kyoto University alloys K3, K5 & K6 in molten fluoride salt (FLiNaK) were also studied (Figure 8). These images were obtained after EIS at 900°C, and showing aggressive corrosion. Comparison of tantalum and ODS ferretic steel corrosion in molten fluoride salt (Figure 9).

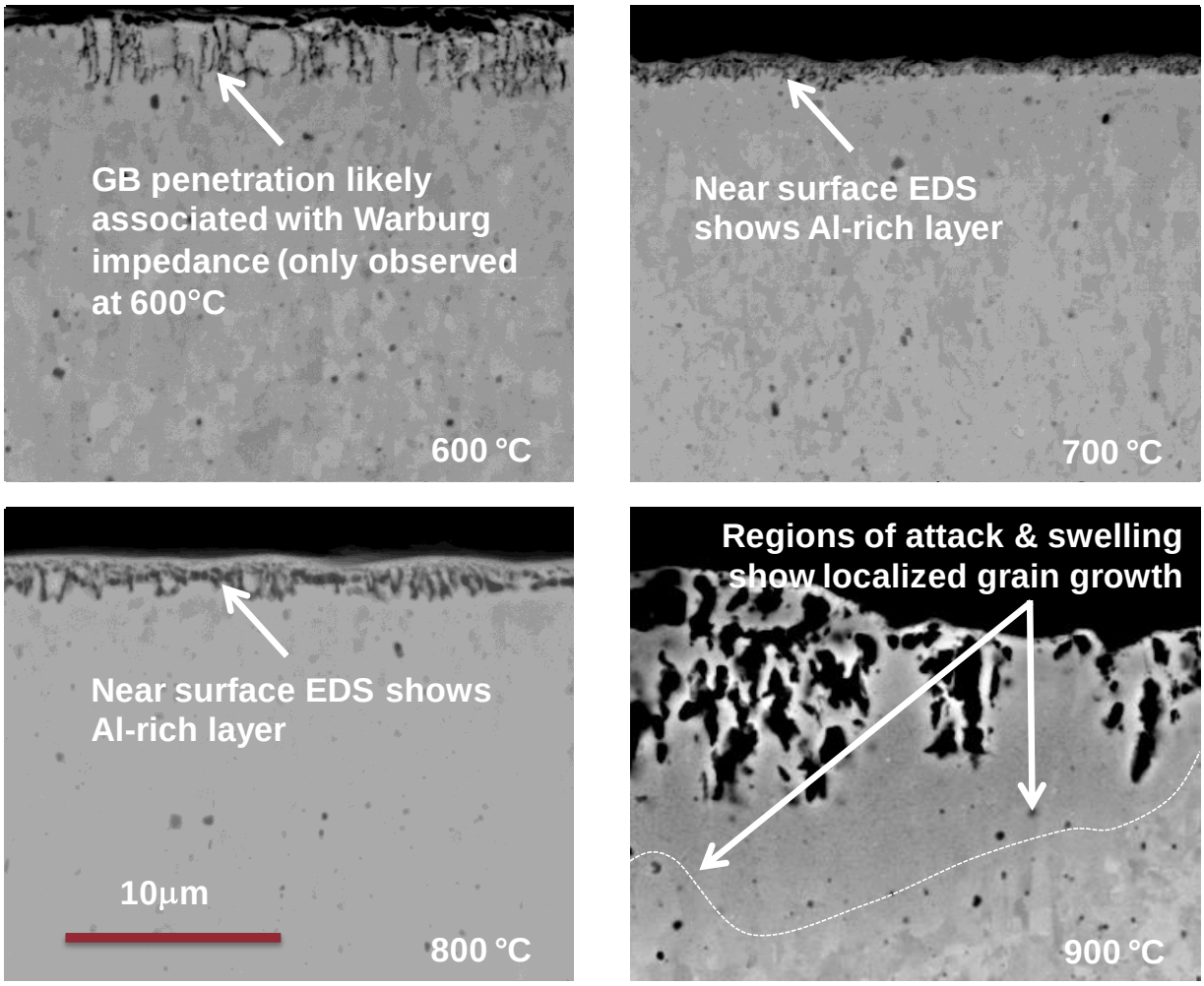

Figure 6 – Electron microscopy of of the ODS-FLiNaK interface has yielded valuable insight into corrosion mechanisms, and temperature-dependent changes in those mechanisms. Dramatic increases in corrosion occur above 800°C.

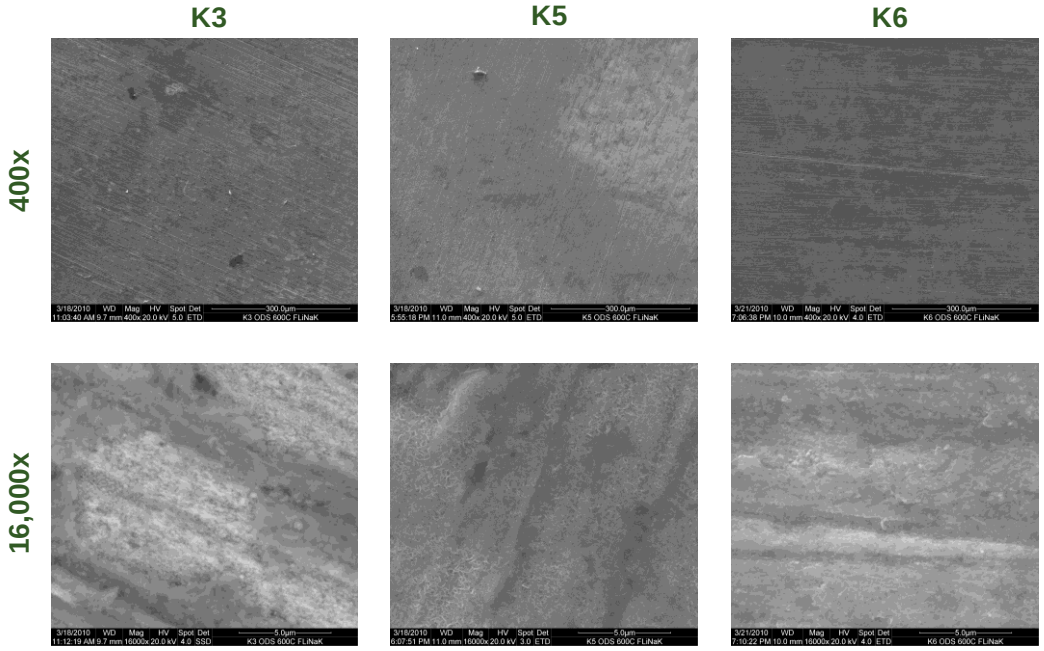

Figure 7 – The corrosion of Kyoto University alloys K3, K5 & K6 in molten fluoride salt (FLiNaK) were also studied. These images were obtained after EIS at 600°C, and show mild corrosion at this temperature, with polishing marks still evident.

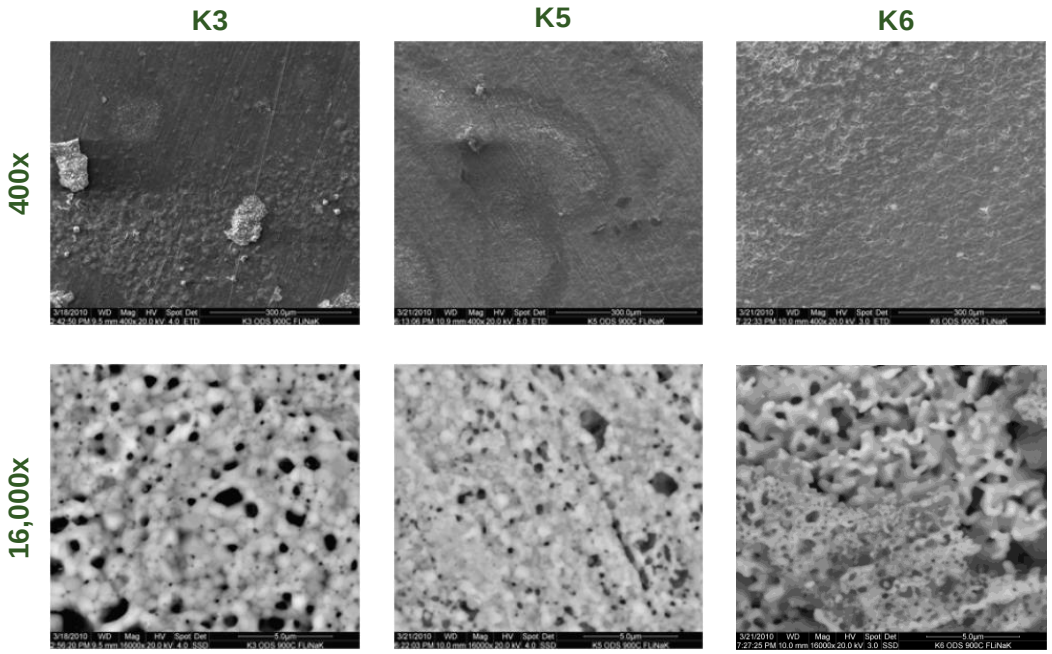

Figure 8 – The corrosion of Kyoto University alloys K3, K5 & K6 in molten fluoride salt (FLiNaK) were also studied. These images were obtained after EIS at 900°C, and showing aggressive corrosion.

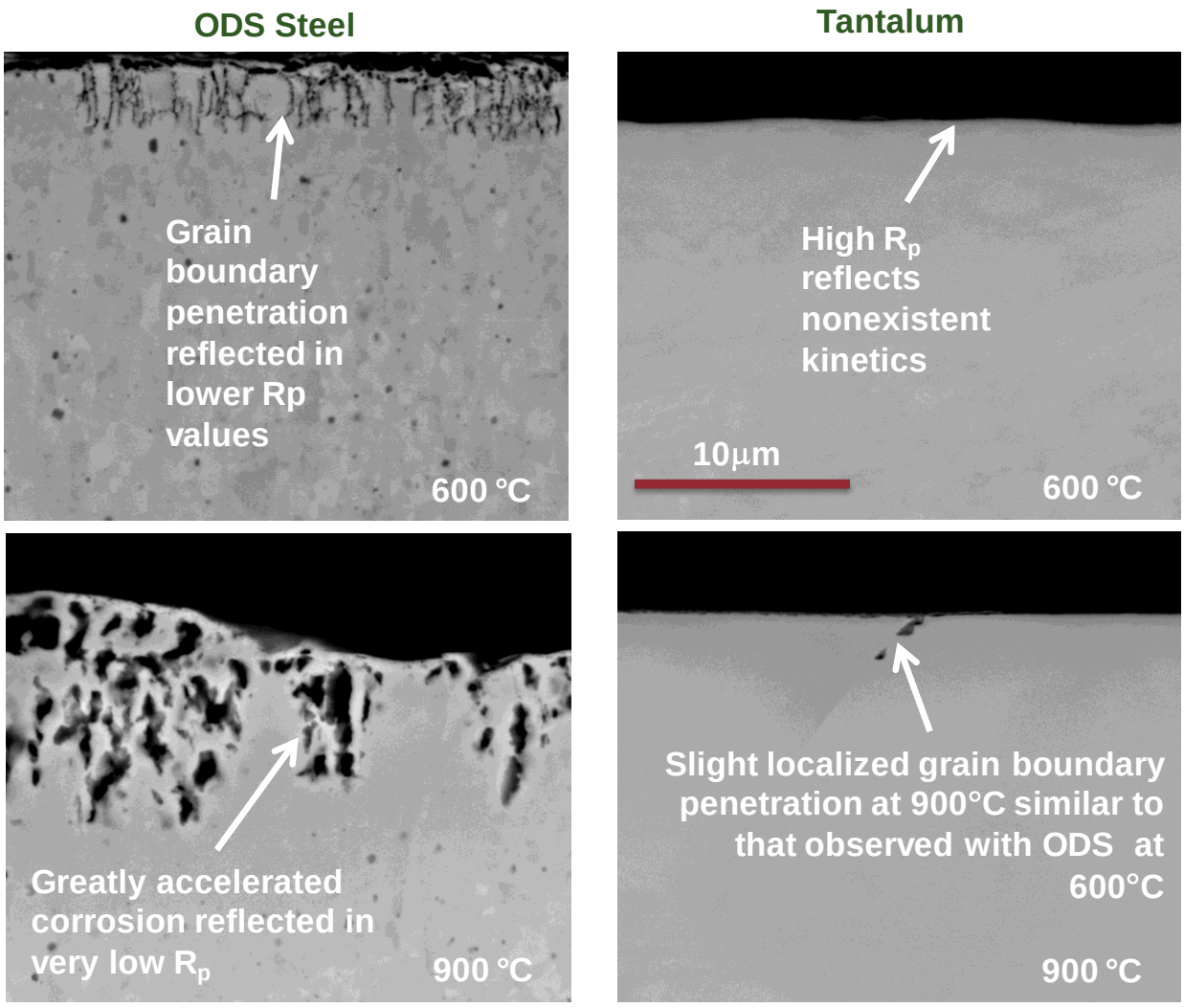

Figure 9 – Comparison of tantalum and ODS ferretic steel corrosion in molten fluoride salt.

Electrochemical impedance spectroscopy has been used to study ODS steels and tantalum alloys in high-temperature molten fluoride salts of importance to future fusion power systems. The three-electrode electrochemical cells shown in Figures 3 and 4 have enabled the corrosion of the ODS steel and tantalum working electrodes with linear polarization and electrochemical impedance spectroscopy (EIS). The working electrodes shown in these figures were subjected to a small amplitude (± 5 mV) potential modulation centered at the open circuit corrosion potential, and the resultant current response measured. The modulation voltage and the current response are separated by a phase angle [12].

The most common equivalent circuit for an electrochemical cell includes the solution resistance, the charge-transfer resistance, the double-layer capacitance and the Warburg impedance associated with mass-transport limitations. Unfortunately, the behavior of a real system may not conform to a simple single-time constant Nyquist or Bode plot. Other effects due to evolving interfacial structure of the corroding sample, including the passive oxide film and the chromium depletion layer, must be captured with additional interfacial impedances to fully explain experimental observations. Additional time constants can be captured by sequentially combining parallel and series impedances until enough complexity has been included to account for observations. The reader is referred to more detailed publications for additional information on materials issues related to fusion and fusion-fission systems, including issues pertaining to corrosion [13-15].

The equivalent circuit model developed to fit the measured impedance spectra is shown in Figure 10. Components at low frequency due to charge transfer associated with corrosion reactions, double layer charging, and mass transfer limitation. At intermediate frequencies, frequency-independent molten fluoride salt resistance is observed. Pseudo inductance due to adsorption or artifact is observed at the highest frequencies. Figures 10 shows the electrochemical impedance spectroscopy from 0.1 to 100,000 Hz during corrosion of ODS steel (MA956) in molten fluoride salts (FLiNaK) at various temperature levels from 600 to 900°C. More specifically, the impedance amplitude (Z) is shown in Figure 11a, while the phase angle (ϕ) is shown in Figure 11b.

The equivalent circuit model, along with the physical meaning of the various equivalent circuit components, is shown in Figure 11. Such models include terms for the ionic conductivity in the molten salt, electron transfer at the electrode-electrolyte interface, the charge separation at immune metal or oxide-covered metal interfaces, and mass-transfer limitations. Quantitative determinations and interpretations of the parameters in the equivalent circuit model, determined from EIS data spanning the frequency range from 0.1 to 100,000 Hz during the corrosion of ODS steel (MA956) in molten fluoride salts (FLiNaK) at various temperature levels from 600 to 900°C are summarized in Table 2. The solution impedance (Rs) independent of temperature; polarization resistance (R_p) increases from 600 to 800°C, as expected with processes involving electrochemical kinetics, but drops precipitously from 800 to 900°C due to change in mechanism; and the Warburg impedance due to diffusion only seen at 600°C. Temperature dependence of circuit elements reveals those associated with corrosive attack are summarized in Figure 13.

The decreased corrosion resistance at 900°C is linked to reduced surface concentration of aluminum, as shown in Figure 14. Quantitative EDS used to estimate near surface concentration of Al. Clear correlation between Al content and R_p observed. This may be either due to complex Al-Cr oxide phase formation and/or effect on near surface grain growth. A comparison of the

corrosion behavior of tantalum and ODS steel (MA956) in molten fluoride salts is shown in Figure 15. Electrochemical impedance spectroscopy from 0.1 to 100,000 Hz during corrosion of tantalum and MA956 ODS steel in molten fluoride salts (FLiNaK) at various temperature levels from 600 to 900°C: (a) impedance amplitude Z and (b) phase angle ϕ.

The interfacial charge-transfer of Ta is significantly higher than ODS steel at 600°C, indicating that tantalum's resistance to corrosive attack by fluoride salt is substantially higher than that of ODS. Corrosion resistance of Ta at 900°C is comparable to that of ODS steel at 600°C. Thus, tantalum cladding may provide an operational margin of approximately 300°C in molten-salt service. High frequency behavior for all samples very nearly the same, with the corresponding active circuit elements not indicative of corrosion.

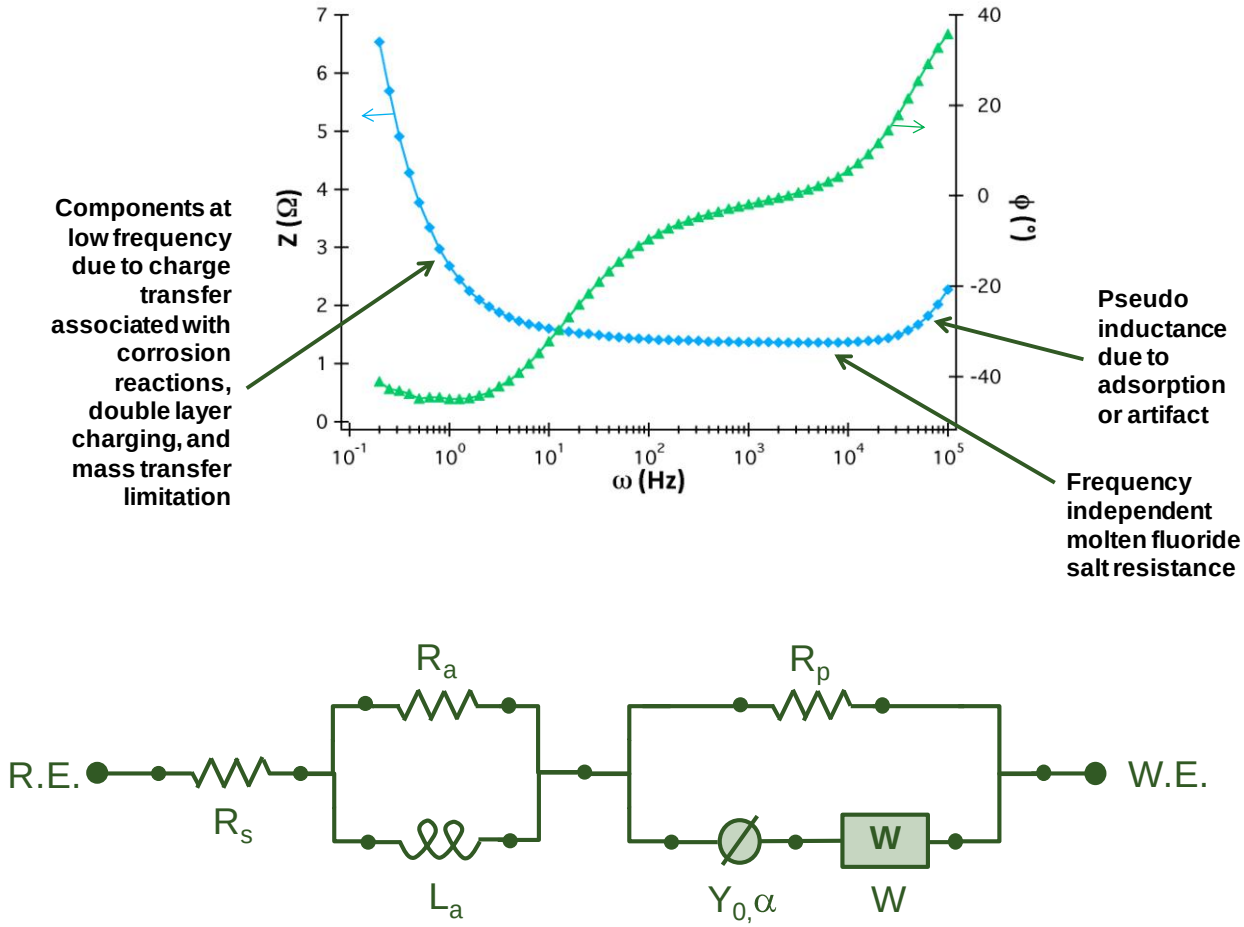

Figure 11 – Equivalent Circuit Model Developed to Fit Impedance Spectra. Components at low frequency due to charge transfer associated with corrosion reactions, double layer charging, and mass transfer limitation. At intermediate frequencies, frequency-independent molten fluoride salt resistance is observed. Pseudo inductance due to adsorption or artifact is observed at the highest frequencies.

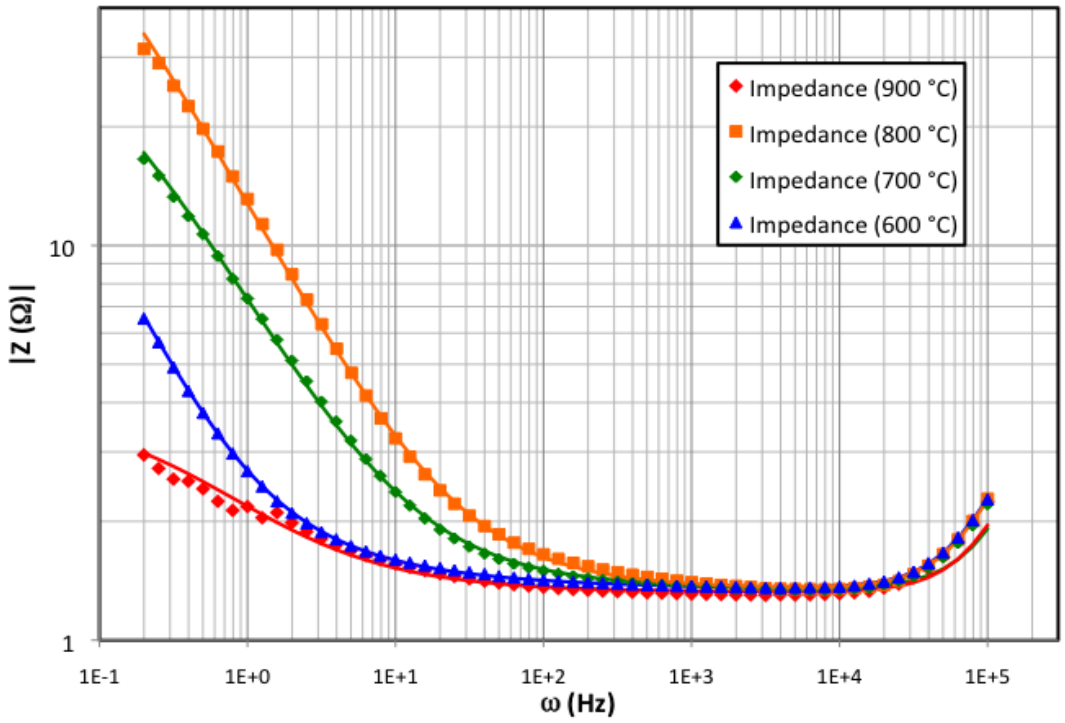

(a)

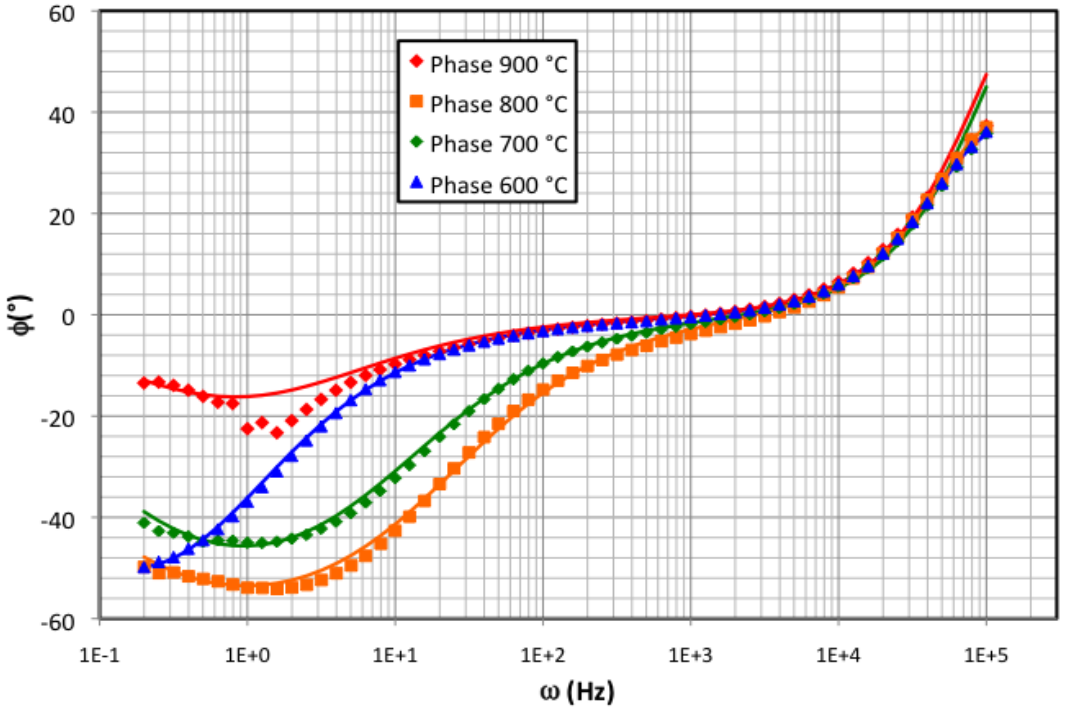

(b)

Figure 12 – Electrochemical impedance spectroscopy from 0.1 to 100,000 Hz during corrosion of ODS steel (MA956) in molten fluoride salts (FLiNaK) at various temperature levels from 600 to 900°C: (a) impedance amplitude Z and (b) phase angle ϕ.

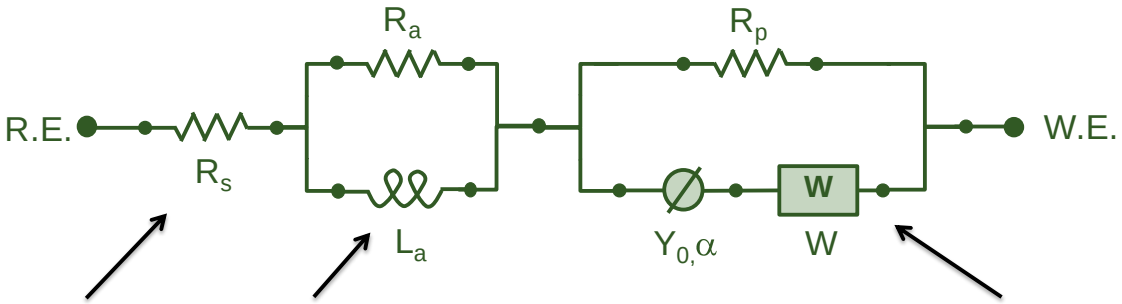

Impedance in Molten Salt

Sole source is resistance to ion transport in molten fluoride salt (R_s)

Expected to be independent of frequency

Weak temperature dependence

Impedance of Inductive Layer

Pseudo inductance:

- Interfacial adsorption processes (L_a & R_a)
- Possible artifact due to electronics and cell design

Impedance of Capacitive Layer

A capacitive double layer is caused by the separation of charges at the electrode surface.

R_p – Polarization resistance reflects charge transfer kinetics associated with anodic and cathodic reactions involved in corrosion process

W – Warburg impedance reflects mass transfer resistance impeding corrosion

Y_0 & α – Reflects double layer charging

Figure 13 – Equivalent circuit model with the physical meaning of the various equivalent circuit components shown. Such models include terms for the ionic conductivity in the molten salt, electron transfer at the electrode-electrolyte interface, the charge separation at immune metal or oxide-covered metal interfaces, and mass-transfer limitations.

Table 2 – Electrochemical impedance spectroscopy from 0.1 to 100,000 Hz during corrosion of ODS steel (MA956) in molten fluoride salts (FLiNaK) at various temperature levels from 600 to 900°C – quantitative determination and interpretation of parameters in equivalent circuit model.

	600 °C	**700 °C**	**800 °C**	**900 °C**
R_s (Ω)	**1.353**	**1.327**	**1.347**	**1.296**
R_p (Ω)	**26.1**	**43.38**	**122.6**	**2.705**
Y_o (…)	**0.1690**	**0.0408**	**0.0216**	**0.2251**
α	**0.9207**	**0.6827**	**0.7079**	**0.6073**
W	**4.67×10^{-1}**	**n/a**	**n/a**	**n/a**
L_a (H)	**2.42×10^{-6}**	**2.31×10^{-6}**	**2.43×10^{-6}**	**2.45×10^{-6}**
R_a (W)	**4.067**	**3.914**	**4.621**	**4.126**

Note: Solution impedance (Rs) independent of temperature; polarization resistance (Rp) increases from 600 to 800°C, as expected with processes involving electrochemical kinetics, but drops precipitously from 800 to 900°C due to change in mechanism; Warburg impedance due to diffusion only seen at 600°C.

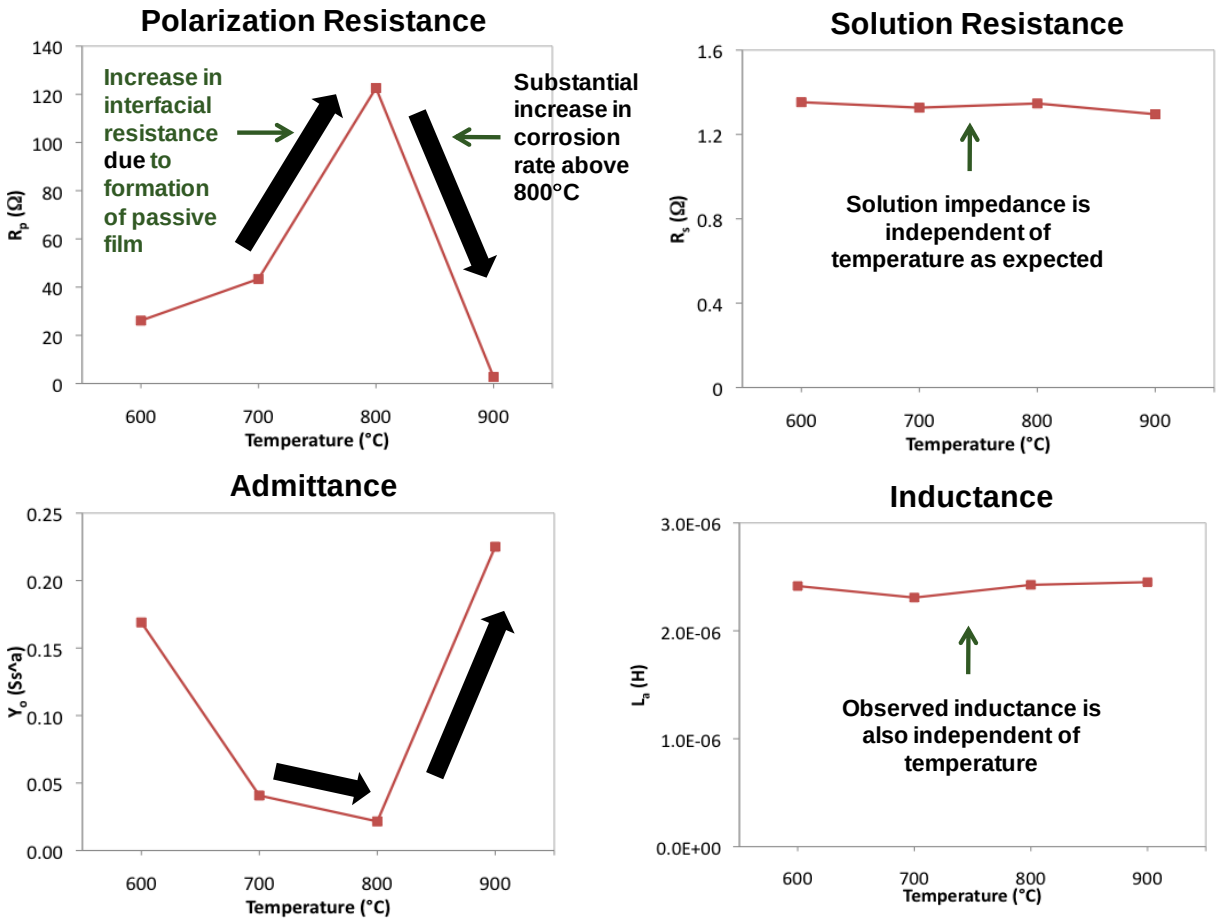

Figure 14 – Temperature dependence of circuit elements reveals those associated with corrosive attack.

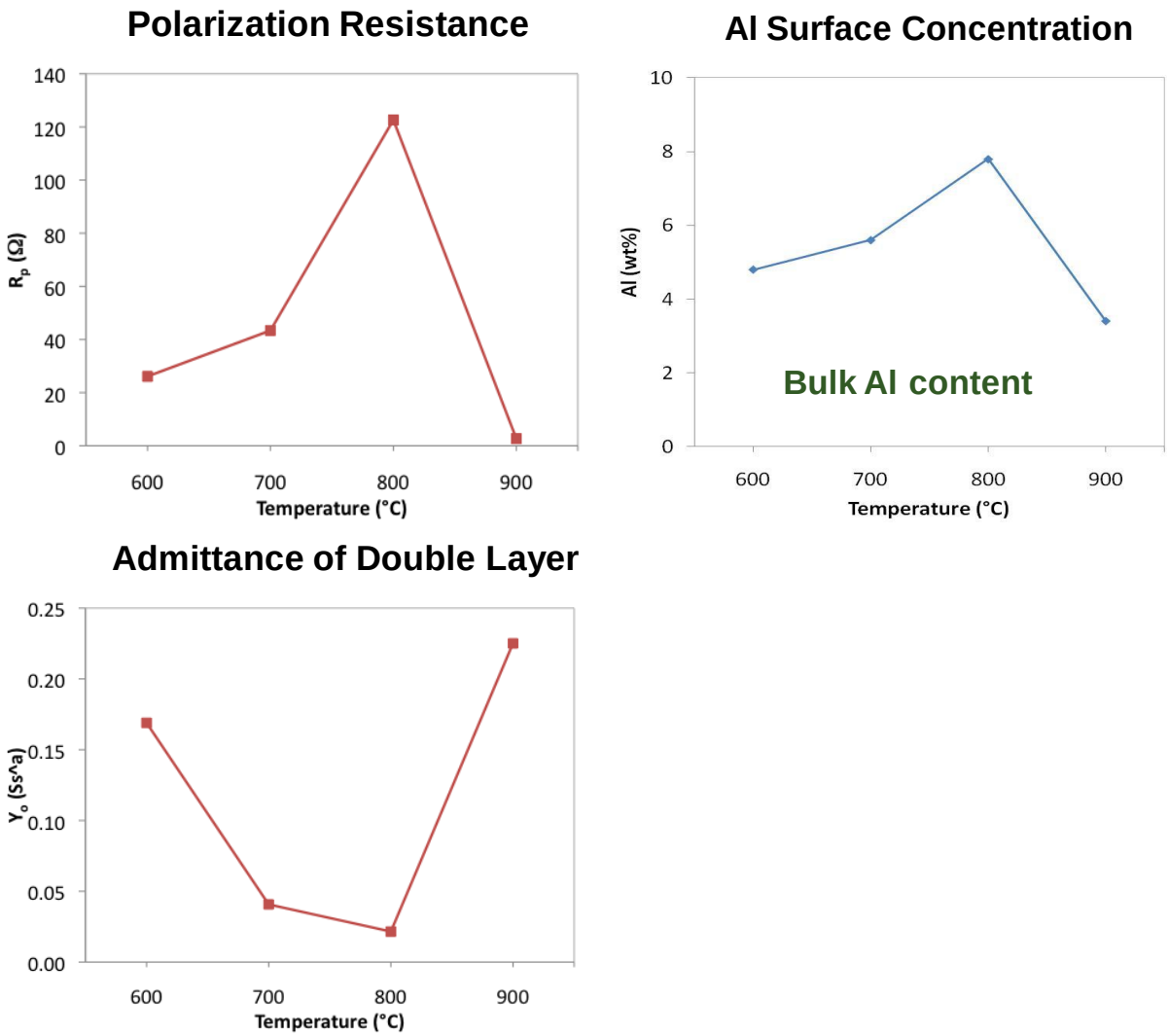

Figure 15 – Decreased Corrosion Resistance at 900°C Linked to Reduced Surface Concentration of Aluminum. Quantitative EDS used to estimate near surface concentration of Al. Clear correlation between Al content and R_p observed. This may be either due to complex Al-Cr oxide phase formation and/or effect on near surface grain growth.

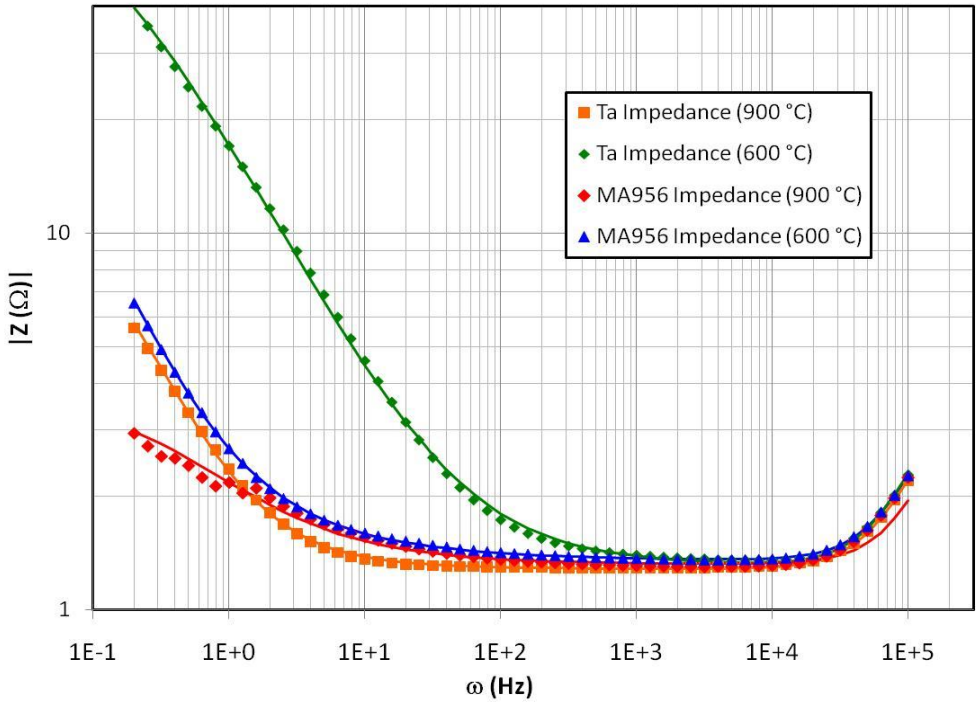

(a)

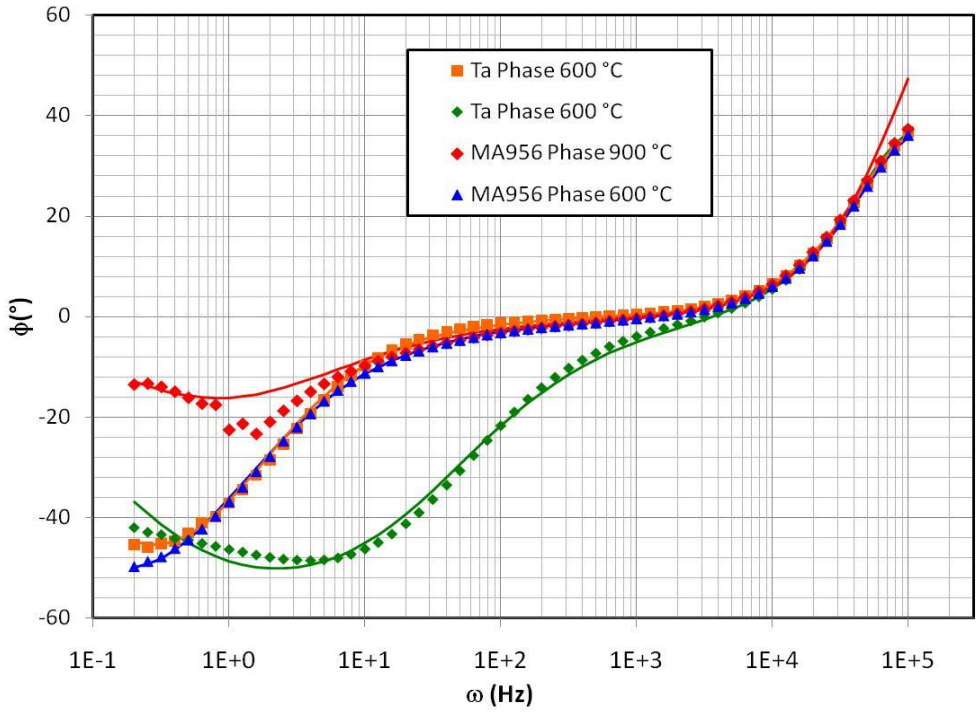

(b)

Figure 16 – A Comparison of the Corrosion Behavior of Tantalum and ODS Steel (MA956) in Molten Fluoride Salts.

DISCUSSION

When two metals are galvanically coupled, an intermediate mixed potential is established. The exact position of this mixed potential, which is located between the oxidation-reduction potentials of the coupled metals, is determined by their relative electrode kinetics. The intersection of the anodic and cathodic Tafel lines identifies the formal mixed potential. This will be the rest potential of both galvanically coupled metals. At this potential, one metal will undergo anodic dissolution, while the other will be cathodically protected, with the possible recombination of hydrogen ions on the surface. By galvanically coupling either metallic lithium or beryllium to iron immersed in a blanket of FLiBe, a mixed potential will be established for the couple between the two reduction-oxidation potentials. The application of mixed potential theory applied to ODS ferritic steel with and without sacrificial beryllium anode in molten Li_2BeF_4 at 815° is shown in Figure 16. This figure clearly shows the cathodic shift of the open circuit corrosion potential due to galvanic coupling of beryllium and ODS steel at 815°C.

Corrosive attack of ODS ferritic steel by Li_2BeF_4 and Li-Na-K-F coolants may be limited by saturation of the electrolyte with dissolved iron and chromium, provided that that continuous precipitation of corrosion products does not occur in cold regions of the system. A simple model has been developed to account for the dissolution of LIFE Engine materials in the high temperature FLiBe and FLiNaK. This model assumes a constant rate of corrosion until the solution becomes saturated with chromium. If the molten salt coolant or fuel saturates with iron and chromium corrosion products, the continued dissolution of the ODS ferritic steel should cease. Figure 17 is a prediction, showing limited corrosive attack of ODS steel by molten salts at T ~ 815°C, assuming a rate of attack of approximately ~5.0 mils per year and a Cr solubility of ~3000 ppm. However, it is important to note that corrosion rates as high as 70.1 mils per year have been reported, and the precipitation of corrosion products at cold locations in a coolant loop could lead to continuous corrosion. Unfortunately, while these materials maintain much of their strength after irradiation at relatively low temperature and dose, they suffer dramatic losses of ductility and become brittle [16]. Furthermore, tantalum alloys may be prone to hydrogen embrittlement phenomena in service with high concentrations of tritium expected in fusion systems.

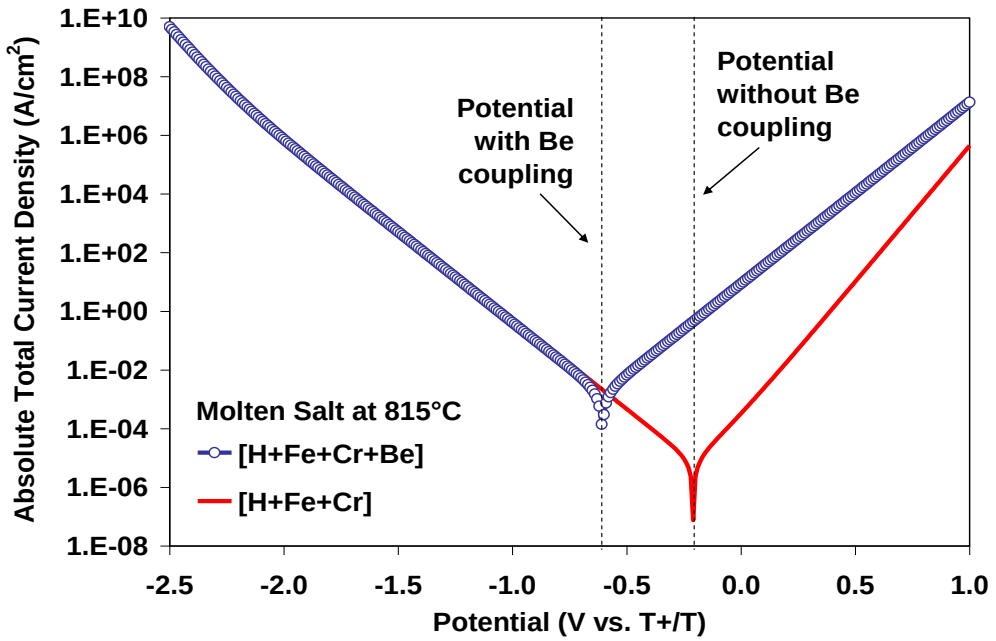

Figure 17 – Mixed potential theory applied to ODS ferritic steel with and without sacrificial beryllium anode in molten Li_2BeF_4 at 815°C.

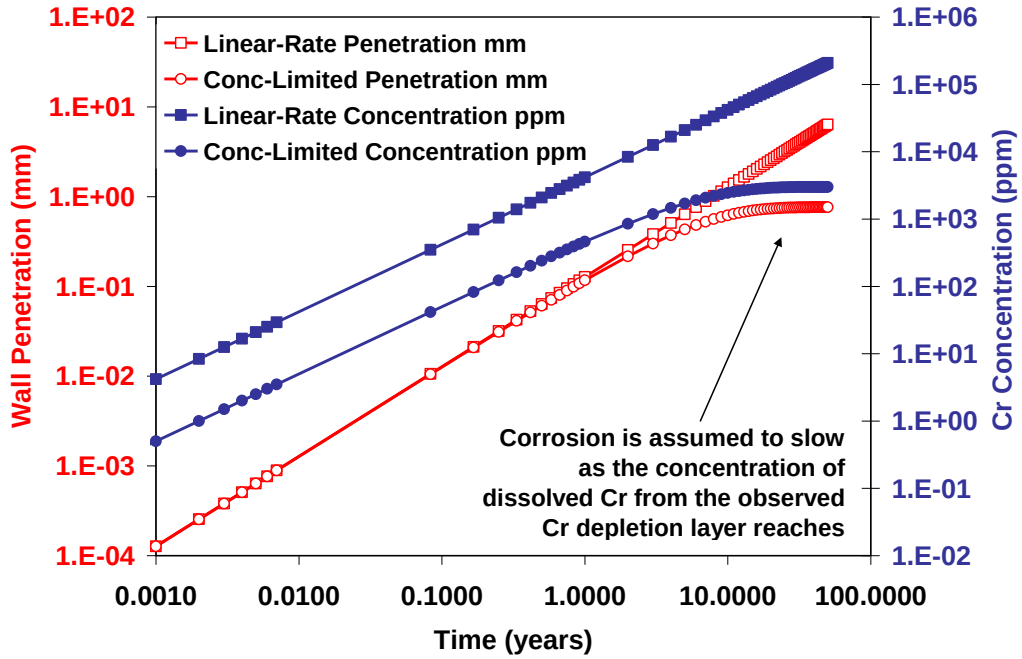

Figure 18 – Corrosion should slow as saturation of chromium is reached in the circulating coolant.

SUMMARY

Alloys such as 12YWT & 14YWT have exceptional high-temperature strength at temperatures greater than 550°C (experts have challenged this material for applications above this level). This class of materials has also demonstrated relatively little radiation induced swelling at damage levels of at least 75 dpa in sodium-cooled fast reactors. However, corrosion of oxide dispersion strengthened (ODS) steels in high temperature molten fluoride salts may limit the life of advanced reactor systems, including some fusion and fusion-fission hybrid systems that are now under consideration.

This paper reports corrosion studies of ODS steel in molten fluoride salts at temperatures ranging from 600 to 900°C. Electrochemical impedance spectroscopy (EIS) was used to measure the temperature dependence of charge transfer kinetics *in situ*, while an environmental electron microscope (ESEM) equipped with energy dispersive spectroscopy (EDS) was used for post-exposure examination of test samples. Alloy MA956 experienced corrosion in the molten fluoride salts at 550 to 900°C, even in carefully controlled glove-box environments with very low levels of oxygen and moisture. The observed rate of attack was found to accelerate dramatically at temperatures above 800°C. Tantalum and tantalum-based alloys such as Ta-1W and Ta-10W have exceptional high temperature strength, far better than ODS steels. Unlike ODS steels, tantalum has been found to exhibit some immunity to corrosive attack by molten fluoride salts at temperatures as high as 900°C, though there is some indication that grain boundary attack may have occurred**.**

ACKNOWLEDGEMENTS

This work was performed under the auspices of the U.S. Department of Energy by Lawrence Livermore National Laboratory under Contract DE-AC52-07NA27344. This work has been supported with Laboratory Directed Research and Development (LDRD) Exploratory Research (ER) funding. The support and leadership of Edward Moses, Tomas Diaz de la Rubia, Judith Kammeraad and Alan Ramponi are gratefully appreciated. Ms. Lesa Christman is thanked for her administrative work in support of this research. This research would have been impossible without her help.

REFERENCES

1. T. R. Allen et al., Nucl. Sci. Eng. 151 (2005) 305–312.
2. S. Ukai et al., J. Nucl. Sci. Tech. 42, 1 (2005) 109-122.
3. R. L. Klueh et al., Nucl. Matls. 367-370 (2007) 48-53.
4. R. Schaublin et al., J. Nucl. Matls. 351 (2006) 247-260.
5. S. Ukai et al., J. Nucl. Matls. 307-311 (2002) 749-757.
6. D. A. Petti et al., Fusion Eng. Des. 81 (2006) 1439-1449.
7. I. N. Sviatoslavsky et al., Fusion Eng. Des. 72 (2004) 307-326.
8. D. F. Williams, ORNL/TM-2006/12, Oak Ridge National Laboratory, 2006.
9. E. T. Cheng et al. Fusion Eng. Des. Fusion Eng. Des. 69 (2003) 205-213.
10. H. Nishimura et al., Fusion Eng. Des. 58-59 (2001) 667-672.
11. J. Farmer, B. El-Dasher, M. Serrano de Caro, J. Ferreira, MRS Symposium Proceedings 1125, PROC-1125-R06-09 (2009) 41-48.
12. A. J. Bard, L. R. Faulkner, Electrochemical Methods, Fundamentals and Applications, John Wiley & Sons, New York, NY, 1980, pp. 44-85; 86-135; 28-315; 316-369.
13. J. C. Farmer, LLNL-TR-407386, Revision 1, October 25th 2008, Lawrence Livermore National Laboratory (DOE Contract DE-AC52-07NA27344), Livermore CA, 170 p.
14. J. C. Farmer, LLNL-TR-408942, November 1st 2008, Lawrence Livermore National Laboratory (DOE Contract DE-AC52-07NA27344), Livermore CA, 92 p.
15. J. C. Farmer, Manuscript 520137, MRS Symposium Q, Scientific Basis for Nuclear Waste Management XXXII, Raul B. Rebak, Neil C. Hyatt, David A. Pickett, Ed., Materials Research Society (MRS) Fall Meeting, December 1st through 5th, 2008, Boston, MA.
16. Thak Sang Byun and Stuart A. Maloy, J. Nuclear Materials 377 (2008) 72-79.